High-pressure synthesis and characterization of $PrMn_7O_{12}$ polymorphs

F. Mezzadri,[1,*] M. Calicchio,[2] E. Gilioli,[2] R. Cabassi,[2] F. Bolzoni,[2] G. Calestani,[1,2] and F. Bissoli[2]
[1]*Dipartimento di Chimica, Università degli Studi di Parma, Area delle Scienze, 43100 Parma, Italy*
[2]*IMEM-CNR, Area delle Scienze 37/A, 43010 Parma, Italy*

(Received 24 July 2008; revised manuscript received 7 November 2008; published 16 January 2009)

We report the synthesis and the characterization of $PrMn_7O_{12}$, a new manganite with multiple (quadruple) perovskite structure of general chemical formula: $AA'_3B_4O_{12}$. This family of manganites is extremely interesting and is attracting a great attention; thanks to its structural peculiarity (and complexity), it might help the comprehension of the ordering phenomena (charge, orbital, spin), which is one of the most challenging issues in the strongly electron correlated rare-earth oxides. Like the majority of the materials having similar structure, $PrMn_7O_{12}$ is a metastable compound, requiring high pressure synthesis. Contrary to other reported isostructural compounds, $PrMn_7O_{12}$ crystallizes in two different forms with rhombohedral (R-3) and monoclinic ($I2/m$) symmetry, the latter characterized by a distortion of the perovskite structure lattice that depends on the synthesis conditions. The approximate stability fields of the two $PrMn_7O_{12}$ phases have been defined in the P/T space, allowing the synthesis of almost single phase samples functional to physical characterization. For the monoclinic phase we succeeded in the growth of crystals sufficiently large to perform structural refinement by single crystal x-ray diffraction data; the rhombohedral structure was instead refined by Rietveld method applied to powder x-ray diffraction data. Although the two phases differ slightly from the crystallographic point of view, physical characterizations reveal surprisingly different properties, in particular for what concerns the magnetic behavior. The differences of the two structures might be explained with a different electronic configuration of Mn, implying the partial occupation of Mn^{3+} in low spin state on the B site of the rhombohedral polymorph.

DOI: 10.1103/PhysRevB.79.014420 PACS number(s): 61.05.cp, 64.70.K−, 61.50.Ks, 75.30.−m

I. INTRODUCTION

$PrMn_7O_{12}$ is a new metastable material, belonging to the family of "quadruple-perovskite" manganites, with general formula $AA'_3B_4O_{12}$, whose structure can usually be derived by doubling the conventional perovskites axes.

The parent compound $NaMn_7O_{12}$ (Ref. 1) can be considered as a model system for the study of the ordering phenomena because the mixed-valence state of the Mn cations is not generated by doping as in the case of the simple perovskites, where the random occupation of the dopant gives rise to structural inhomogeneities. On the contrary, in these compounds, every Mn ion occupies a different crystallographic site; this feature allows the direct observation of the charge/orbital/spin orderings. The formula of $NaMn_7O_{12}$ is often written as $(NaMn^{3+}{}_3)(Mn^{3+}{}_2Mn^{4+}{}_2)O_{12}$ to explicit the relationship with the perovskite structure and to define the Mn valence distribution between the A' and B sites.

This family of compounds is truly fascinating from the structural point of view: it is based on a 3D network of corner-sharing MnO_6 tilted octahedra, centered on the B site; such a highly distorted structure, can only be accommodated under high pressure by the presence of a Jahn-Teller atom (Mn^{3+} or Cu^{2+}) on the A' site, with formal square planar coordination [coordination number (CN)=4], due to large distortion of the standard icosahedral coordination (CN =12), typical of the A site.

The occupation of the A site determines the properties of the compounds. By selecting an appropriate monovalent [(Na^+, $NaMn_7O_{12}$ (Ref. 1)], divalent [(Ca^{2+}, $CaMn_7O_{12}$ (Ref. 2)], trivalent [(La^{3+}, $LaMn_7O_{12}$ (Ref. 3)], or even tetravalent cation (Th^{4+}, $ThCu_3Mn_4O_{12}$,[4] which can only be stabilized by Cu^{2+} as a Jahn-Teller cation in the A' site), one can modify the Mn^{3+}/Mn^{4+} ratio in the B site of the structure and consequently change the ordering phenomena. As far as the structure is concerned, the size of the A cation obviously influences the distortion; this can be easily understood by recalling the geometric tolerance factor [$t=(A\text{-O})/\sqrt{2}(\text{Mn-O})$],[5] describing the mismatch of adjacent layers in pseudocubic perovskites. The t value is generally <1, and can be accommodated by a cooperative tilting of the MnO_6 octahedra, deviating the Mn-O-Mn bond angle from 180°. This angle can be taken as a parameter controlling the interatomic interactions; it can be modified by the A-cation size and by external stimuli (e.g., hydrostatic pressure), and clearly affects the material electronic properties.[6]

Among the various compounds, the ones with a trivalent occupation of the A site are of particular interest since they should not exhibit charge ordering (all Mn atoms are in 3+ valence state), while keeping the same structure of $NaMn_7O_{12}$. Recently, neutron diffraction data of $LaMn_7O_{12}$ have been collected,[3] showing a very complex magnetic behavior, due to the cooperative Jahn-Teller distortion of the Mn^{3+} occupying different sublattices.

In order to clarify some differences between mixed-valent manganite ($NaMn_7O_{12}$-like) and isovalent compound ($LaMn_7O_{12}$-like), and to better understand the controversial issue of the ordering phenomena, we attempted to synthesize $PrMn_7O_{12}$. On one hand, differently from La, Pr is magnetically active. Besides, it is not a pure trivalent cation, being also Pr^{4+} a (less) stable form. $ThCu_3Mn_4O_{12}$ (Ref. 7) is so far the unique $AA'_3B_4O_{12}$ compound containing a tetravalent ion on the A site reported in literature and the presence of Cu^{2+} in A' seems to play an important role in stabilizing the struc-

ture. Therefore, it is interesting to study $PrMn_7O_{12}$, even in order to analyze the resulting Pr and Mn valence, and its effect on structural and magnetic properties.

$PrMn_7O_{12}$ can be obtained by high pressure synthesis in two different forms, with monoclinic and rhombohedral (trigonal) symmetry, both metastable at room temperature (RT); although the occurrence of polymorphism has been reported in this family of compounds (a reversible cubic-monoclinic transition occurs in $NaMn_7O_{12}$ at 176 K), the coexistence of two different phases has never been observed previously. Interestingly, the monoclinic phase displays a variable structural distortion (with respect to the idealized cubic structure) as a function of the synthesis conditions.

The approximate stability fields of both $PrMn_7O_{12}$ phases have been defined in the P/T space and the two structures have been refined by powder x-ray diffraction (XRD). Small single crystals (50–100 μm size) of the monoclinic polymorph have been grown in a few experiments, making available structural refinement from single crystal XRD data. Although the synthesis conditions differ only slightly, the two phases can be obtained in an almost pure form, allowing a detailed thermal [differential scanning calorimetry (DSC)], electrical [$R(T)$], and magnetic [superconducting quantum interference device (SQUID)] characterization. Structural analyses demonstrate that $PrMn_7O_{12}$ polymorphs only differ for the type of distortion, while Pr (and Mn, as well) are present in their trivalent configuration, in tight analogy with the counterpart $LaMn_7O_{12}$.

II. APPARATUS AND EXPERIMENTAL

The synthesis of $PrMn_7O_{12}$ takes place under high pressure/high temperature (HP/HT) conditions, using a commercial 6/8 multianvil apparatus (Rockland) with tungsten carbide cubes, Cr_2O_3-doped MgO octahedra and graphite furnace. Details of the synthesis procedures have been reported elsewhere.[8] In some experiments the assembly is mounted with two or three capsules, each one filled with a different precursor, in order to carry out two or more reactions under identical conditions. Calibration experiments carried out on standard materials show that the temperature and pressure gradients inside the capsule can be considered negligible at the working conditions.

Stoichiometric and 5–20 mol % Pr-rich mixtures of Mn-oxides (MnO_2 Alfa Aesar, 99.9% and Mn_2O_3 Ventron, 98%) and Pr_6O_{11} (Aldrich, 99.9%) are used as reagents.

The reagents are mixed, finely grounded in a glove box to prevent hydration, and encapsulated in the Pt foils, without any welding. The pressure is first increased up to the maximum value at the rate of 160 bar/min. The capsule is then heated up to the maximum temperature at a rate of 50 °C/min, kept for 2 h, and quenched to room temperature by switching off the heater. Finally, the pressure is released at ≈50 bar/min.

$PrMn_7O_{12}$ looks like a dark-gray compact and homogeneous material.

Powder XRD patterns were collected using Cu $K\alpha$ radiation ($\lambda = 1.54178$ Å) with a Thermo ARL X'tra powder diffractometer equipped with a Thermo Electron solid state detector to eliminate the incoherent background produced by fluorescence of manganese. Data were collected with 0.02° 2θ steps and counting time ranging from 2 to 10 s/step. Structure refinement were performed with GSAS.[9] Single crystal XRD data were collected with Mo $K\alpha$ ($\lambda = 0.71069$ Å) radiation on a Bruker AXS Smart diffractometer, equipped with a charge-coupled device (CCD) area detector. The data for the structural refinement were collected at room temperature on single crystals mechanically separated from the powders.

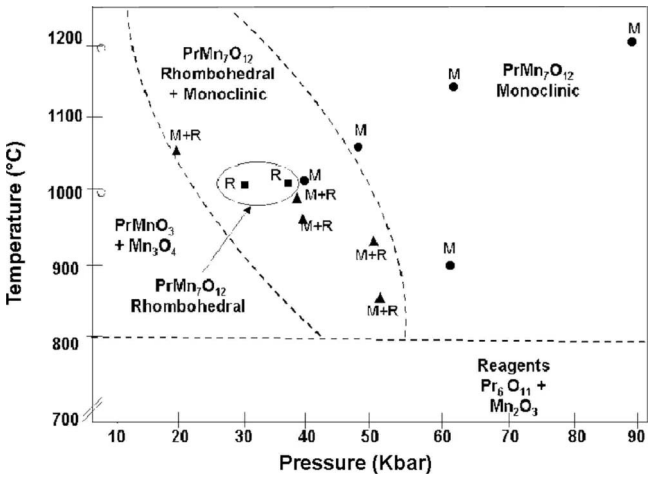

FIG. 1. $PrMn_7O_{12}$ phase diagram in the P/T space.

Differential scanning calorimetry measurements were performed with a Perkin-Elmer 7 apparatus using heating/cooling rates ranging from 10 to 20 °C min^{-1}. The magnetic properties of $PrMn_7O_{12}$ have been studied using a Quantum Design SQUID magnetometer in the temperature range 5–300 K and applied magnetic field up to 5.5 T. dc resistivity $R(T)$ has been measured by standard four-probe method from 77 to 300 K using a close cycle cryostat.

III. RESULTS AND DISCUSSION

A. Phase diagram

Several experiments have been performed in the pressure range: 30–90 kbar and temperature range of 700–1200 °C, while the reaction time has been kept constant to 2 h. By analyzing the reaction products by powder XRD, in search of the optimal synthesis conditions, we found that $PrMn_7O_{12}$ crystallizes in two phases, identified as monoclinic (space group *n*.12, *I*2/*m*) and rhombohedral (space group *n*.148, *R*-3). Although a precise determination of the $PrMn_7O_{12}$ phase stability fields is beyond the scope of this paper, a preliminary P/T phase diagram of $PrMn_7O_{12}$, as determined in this work, is presented in Fig. 1. The monoclinic polymorph forms at higher pressure, while at lower pressure there is coexistence of the two phases. This is in contrast with simple considerations based on the structure densities: being the rhombohedral $PrMn_7O_{12}$ slightly denser than the monoclinic one, as discussed in the following, one can conclude that the volume reduction under increasing pressure is not the driving force to the formation of the two phases.

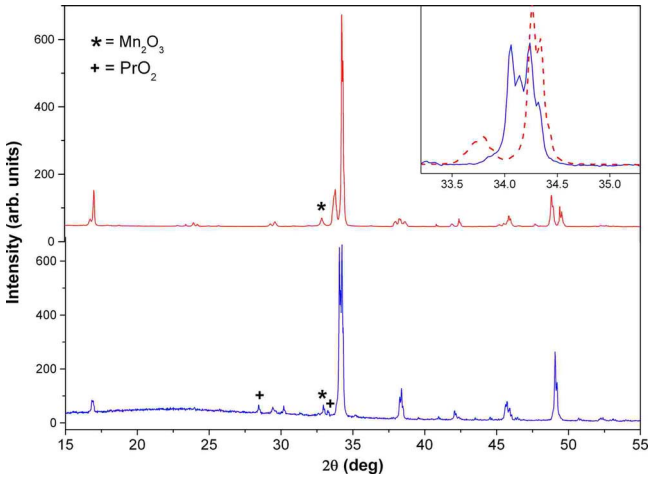

FIG. 2. (Color online) Powder XRD pattern of monoclinic (red, top) and rhombohedral (blue, bottom) $PrMn_7O_{12}$. Impurities phases are marked with symbols. The inset shows the 2θ range of 33.0°–35.5°, particularly indicative for the detection of rhombohedral (blue, straight line) and monoclinic (red, dotted line) phases.

The powder XRD data analysis evidences that the samples are almost single phase (>96%), Mn_2O_3 (ICSD chart No. 71-0635), Mn_3O_4 (ICSD chart No. 75-1560), and PrO_2 (ICSD chart No. 75-0152), being the main impurities. XRD patterns of both rhombohedral and monoclinic phases are reported in Fig. 2. The distortion of the monoclinic structure is variable; higher reaction temperatures produce higher volume, with densities values decreasing from 5.79 g/cm^3 (T=1200 °C) to 5.74 (T=900 °C). The value d =5.77 g/cm^3 refers to a particularly pure monoclinic sample, taken as reference, thereinafter denoted as (I). Pressure has a negligible effect on the distortion. In Fig. 3 the powder XRD data relative to samples grown in different conditions are shown. The reported 2θ range refers to the family of reflections −202, 022, 220, 202 (left to right) that are

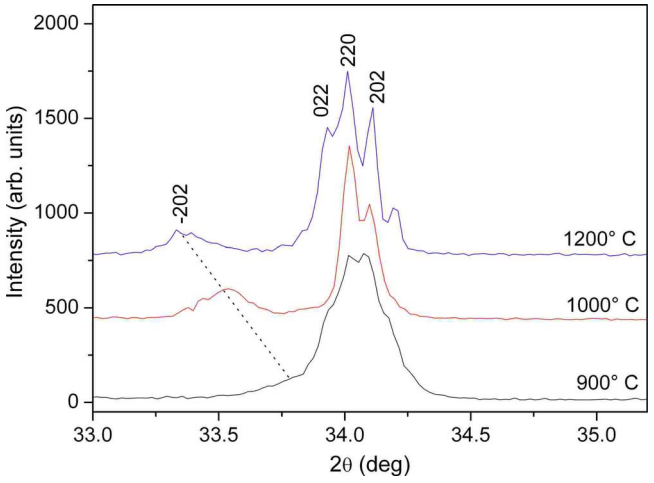

FIG. 3. (Color online) Powder XRD patterns, in the 2θ range 33.0°–35.5°, of monoclinic $PrMn_7O_{12}$ samples synthesized at different temperatures. The monoclinic cell shows different distortions as a function of synthesis conditions; dotted line is a guide for the eyes and follows the deviation of β from 90°.

indicative of both the deviation of β angle from 90°, evidenced by a shift of the −202 reflection toward lower 2θ values, and of the metrical relationship between the cell parameters. The −202 peak appears particularly broad, suggesting the presence of crystals with slightly different distortion within the same synthesis batch.

In order to follow the evolution of the distortion, several $PrMn_7O_{12}$ samples have been postannealed under different conditions and then analyzed by XRD and DSC. $PrMn_7O_{12}$ completely decomposes at 800 °C if thermal treatment is carried out at room pressure in N_2 atmosphere yielding Mn and Pr oxides and the simple perovskite $PrMnO_3$. When the annealing process takes place in air, the decomposition begins at about 900 °C.

The crystal structure of the monoclinic phase is modified by thermal posttreatments of the as-prepared samples, causing simultaneously the increase of the distortion (β angle) and the expansion of the cell volume (lattice parameters) with increasing temperature and annealing time; the latter variable increases β until its limit value for each defined temperature of treatment. This behavior follows the tendency observed in as synthesized samples (Fig. 3). The monoclinic cell parameters, determined by the synthesis temperature or by a subsequent annealing, do not vary substantially during the cooling process, revealing that the process originating the increase in the monoclinic distortion is irreversible.

Pure rhombohedral phase has been experimentally found only in a very limited region of the P/T phase diagram, within the region of coexistence of the two polymorphs; interestingly, it is possible to obtain almost pure samples of both phase under similar conditions ($P \approx 40$ kbar and T =970–1000 °C). As frequently happens in metastable materials,[10] this suggest that the $PrMn_7O_{12}$ system possesses slightly different Gibbs free energy minima, and it can fall down to one or another minima (rhombohedral or monoclinic structure) with small variations in the synthesis conditions.

Differently from the monoclinic case, no variation in the structural parameters of the rhombohedral phase was observed by changing the synthesis conditions. However thermal treatments of rhombohedral samples produce an irreversible phase transition to monoclinic symmetry when the sample is heated above 700 K. In relation to this phase transition, DSC measurements performed on heating evidenced an endothermic peak (21.96 kJ mol^{-1}) with the onset at 714 K.

B. Structural refinements and thermal analysis

Small crystals (50–100 μm) of the monoclinic polymorph were obtained in different experiments and, mechanically isolated from the reacted mass, were studied by single crystal XRD. The results confirmed the variability of the monoclinic structure. We report here detailed structural information concerning two different monoclinic samples, identified by (I) and (II); the first is associated to the reference sample as previously defined, while the second is the one presenting the maximum observed distortion. In both cases the structure was solved with SIR2002 (Ref. 11) and

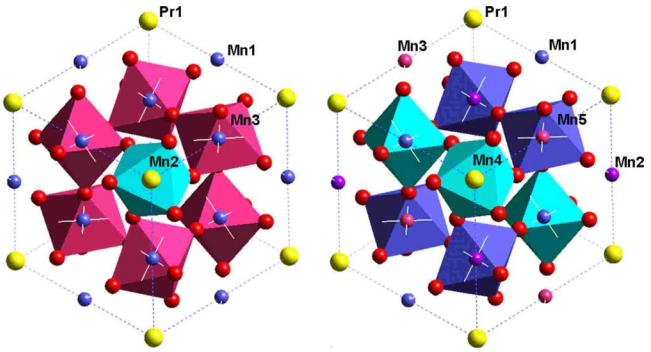

FIG. 4. (Color online) Rhombohedral (left) and monoclinic (right) structure viewed along the [111] direction in terms of pseudocubic perovskite cell. Symmetry-equivalent cations are identified by the same colors (gray tones).

refined with SHELX97 (Ref. 12) software making use of anisotropic thermal parameters for all atoms. The rhombohedral and monoclinic structures are represented in Fig. 4. For what concerns the rhombohedral phase, no crystal of sufficient dimension was obtained in spite of several attempts and the structure was refined by Rietveld analysis carried out on powder XRD data using GSAS.[9,13] The results of the structural refinements are reported in Table I. The Mn-O bond lengths and angles, derived from structural refinement, are reported in Table II together with Jahn-Teller distortion parameters and ionic charges. Atomic oxidation states were calculated using CHARDIS99, a program used to compute charge distributions and bond valence in nonmolecular crystalline structures.[14] The results given by CHARDIS indicate 3+ oxidation state for Mn and Pr, in analogy with $LaMn_7O_{12}$, in both rhombohedral and monoclinic phases. Therefore, we conclude that the presence of different structures cannot be ascribed to different cationic valence states. As shown in Table II, the average Mn-O distances of corresponding manganese atoms are comparable in monoclinic and rhombohedral structures. In the monoclinic phase the distortion of the MnO_6 octahedra observed on both $B1$ and $B2$ sites can be considered the fingerprint of the Jahn-Teller effect generated by Mn^{3+} ions in high spin configuration. This feature leads to the definition of an orbital ordered system, in which the magnetic moments of Mn atoms form ferromagnetic sheets in the ac plane that are antiferromagnetically coupled along the b axis in a A-type structure.[15] It is interesting to note that variation in the structural distortion, observed passing from I to II, is mostly connected with the deformation of the MnO_6 octahedra centered on the B sites (see σ_{JT} in Table II), while the Mn(B)-O-Mn(B) angles and the cell volumes remain substantially the same. On the other hand in the rhombohedral polymorph, which is isostructural with $CaMn_7O_{12}$,[2] only the $B2$ site shows a distorted octahedral environment, whereas the $B1$ manganese atom lies on a site with -3 symmetry, forcing all the distances of the corresponding MnO_6 octahedron to be equal. In $CaMn_7O_{12}$ the latter site is occupied by Mn^{4+} and the rhombohedral symmetry accommodate in the

TABLE I. Crystal data and refinement parameters for rhombohedral and monoclinic $PrMn_7O_{12}$. The cationic site definition corresponds to the formula $AA'_3B_4O_{12}$. U_{eq} is defined as one third of the trace of the orthogonalized U_{ij} tensor.

$PrMn_7O_{12}$ rhombohedral					$PrMn_7O_{12}$ monoclinic (I)					$PrMn_7O_{12}$ Monoclinic (II)				
Space group 148 (R-3)					Space group 12 ($I2/m$)					Space group 12 ($I2/m$)				
$a=b=c=6.435(1)$ Å					$a=7.480(1)$, $b=7.385(1)$, $c=7.474(1)$ Å					$a=7.498(1)$, $b=7.377(1)$, $c=7.473(1)$ Å				
$\alpha=\beta=\gamma=109.60(1)°$					$\beta=90.96(1)°$					$\beta=91.25(2)°$				
$V=204.11(6)$ Å^3 ($Z=1$)					$V=412.82(5)$ Å^3 ($Z=2$)					$V=413.24(10)$ Å^3 ($Z=2$)				
$d=5.84$ g/cm^3					$d=5.77$ g/cm^3					$d=5.76$ g/cm^3				
Atom (site)	x	y	z	U_{iso}(Å^2)	Atom (site)	x	y	z	U_{eq}(Å^2)	Atom (site)	x	y	z	U_{eq}(Å^2)
Pr(A)	0	0	0	0.0237(8)	Pr(A)	0	0	0	0.0111(2)	Pr(A)	0	0	0	0.0070(1)
Mn1(A′)	0	$\frac{1}{2}$	$\frac{1}{2}$	0.0098(5)	Mn1(A′)	$\frac{1}{2}$	$\frac{1}{2}$	0	0.0135(2)	Mn1(A′)	$\frac{1}{2}$	$\frac{1}{2}$	0	0.0071(2)
Mn2(B1)	$\frac{1}{2}$	$\frac{1}{2}$	$\frac{1}{2}$	0.0098(5)	Mn2(A′)	$\frac{1}{2}$	0	0	0.0130(2)	Mn2(A′)	$\frac{1}{2}$	0	0	0.0076(2)
Mn3(B2)	$\frac{1}{2}$	0	0	0.0098(5)	Mn3(A′)	0	$\frac{1}{2}$	0	0.0095(2)	Mn3(A′)	0	$\frac{1}{2}$	0	0.0041(1)
O1	0.860(3)	0.700(2)	0.184(3)	0.0150(20)	Mn4(B1)	$\frac{3}{4}$	$\frac{3}{4}$	$\frac{1}{4}$	0.0127(2)	Mn4(B1)	$\frac{3}{4}$	$\frac{3}{4}$	$\frac{1}{4}$	0.0068(2)
O2	0.530(3)	0.692(3)	0.825(4)	0.0150(20)	Mn5(B2)	$\frac{3}{4}$	$\frac{3}{4}$	$\frac{3}{4}$	0.0094(2)	Mn5(B2)	$\frac{3}{4}$	$\frac{3}{4}$	$\frac{3}{4}$	0.0041(1)
					O1	0.0081(2)	0.6901(2)	0.8266(2)	0.0155(4)	O1	−0.0151(2)	0.6907(2)	0.8276(2)	0.0074(3)
					O2	0.8295(3)	0	0.3081(3)	0.0152(5)	O2	0.8197(3)	0	0.3144(3)	0.0088(4)
					O3	0.6778(3)	$\frac{1}{2}$	0.8120(3)	0.0146(5)	O3	0.6670(3)	$\frac{1}{2}$	0.8051(3)	0.0078(4)
					O4	0.6890(2)	0.8253(2)	0.9945(2)	0.0160(4)	O4	0.6880(2)	0.8247(2)	0.9866(2)	0.0087(3)
Nobs=386					485 unique reflections					648 unique reflections				
No. of parameters=33					No. of free parameters=60					No. of free parameters=60				
$R(F^2)=0.0860$					GooF=1.119					GooF=1.068				
Rp=0.0922					$R_1=0.0179$					$R_1=0.0205$				
wRp=0.1309					$wR_2=0.0490$					$wR_2=0.0500$				

TABLE II. Selected bond lengths (Å) and angles (deg), octahedral distortion parameters and ionic charges for Mn atoms in rhombohedral and monoclinic $PrMn_7O_{12}$. $\sigma_{JT}=\sqrt{1/3\Sigma_i[(d_{Mn\text{-}O})_i-(d_{Mn\text{-}O})]^2}$ is a measure of the octahedral distortion from Ref. 27.

Rhombohedral, *R*-3						
	A′ site		B1 site	B2 site		Angle
Mn1-O1	2×1.887(12)	Mn2-O2	6×1.940(20)	Mn3-O1	2×1.907(13)	Mn2-O1-Mn3	12×137.7(5)
Mn1-O2	2×1.937(23)			Mn3-O2	2×2.037(21)		
				Mn3-O1	2×2.086(19)		
Average	1.912(18)		1.940(20)		2.010(18)		137.7(5)
σ_{JT} (×10^2)			0		11		
Charge	3.00		3.12		2.96		

Monoclinic (I), *I*2/*m*							
	A′ site		B1 site		B2 site		Angle
Mn1-O2	2×1.903(2)	Mn4-O1	2×1.958(2)	Mn5-O4	2×1.971(2)	Mn5-O4-Mn4	4×137.9(1)
Mn1-O3	2×1.951(2)	Mn4-O2	2×1.986(1)	Mn5-O3	2×1.981(1)		
		Mn4-O4	2×2.034(2)	Mn5-O1	2×2.053(1)	Mn4-O1-Mn5	4×137.7(1)
Mn2-O4	4×1.915(2)						
						Mn4-O2-Mn4	2×136.8(1)
Mn3-O1	4×1.913(2)						
						Mn5-O3-Mn5	2×137.5(1)
Average	1.918(2)		1.993(2)		2.001(1)		137.6(1)
σ_{JT} (×10^2)			4		5		
Charge	3.00		2.98		3.02		

Monoclinic (II), *I*2/*m*							
	A′ site		B1 site		B2 site		Angle
Mn1-O2	2×1.915(2)	Mn4-O4	2×1.900(1)	Mn5-O1	2×1.893(1)	Mn5-O4-Mn4	4×137.7(1)
Mn1-O3	2×1.941(2)	Mn4-O2	2×1.974(1)	Mn5-O3	2×1.992(1)		
		Mn4-O1	2×2.129(1)	Mn5-O4	2×2.105(1)	Mn4-O1-Mn5	4×137.5(1)
Mn2-O4	4×1.914(1)						
						Mn4-O2-Mn4	2×138.3(1)
Mn3-O1	4×1.909(1)						
						Mn5-O3-Mn5	2×135.5(1)
Average	1.918(1)		2.001(1)		1.997(1)		137.4(1)
σ_{JT} (×10^2)			13		12		
Charge	3.00		2.99		3.01		

B sites Mn^{4+} and Mn^{3+} ions in the stoichiometric 1:3 ratio deriving from the presence of Ca^{2+} in the *A* site of the structure. In $PrMn_7O_{12}$, the eventual existence of Mn^{4+}, when related to oxygen nonstoichiometry, should derive from the presence of interstitial extraoxygen. Whereas oxygen deficiency is well known in perovskites (until to the limit case of the infinite-layer materials, i.e., $CaCuO_2$ and related phases), ABO_{3+x} systems have never been reported. In fact, being the perovskite a very dense structure, no interstitial site that could be occupied by extraoxygen exists in the lattice. The presence of extraoxygen has been reported only for perovskite-related structures containing a double AO layer in the stacking sequence, a necessary condition to create interstitial sites in these structures. As a conclusion, our compound could be eventually oxygen deficient, but not oxygen rich, so that the presence of Mn^{2+} (but not of Mn^{4+}) could be hypothesized. However, the presence of the large divalent cation is definitively ruled out by the structure analysis. The presence of Mn^{4+} could be produced, on the side, by cationic deficiency, in particular by Pr^{3+} deficiency. This has been taken into account in refining the structure. However, since the refined fraction was close to the full occupancy within the e.s.d., the Pr site was considered full occupied in the final refinement cycles. This agrees with the results of other struc-

tural studies, which pointed out a stoichiometric composition for all the members of the AMn_7O_{12} family previously investigated. Therefore the presence of Mn^{4+} was ruled out on the basis of our powder XRD data refinements. Moreover, being Mn^{3+} the only manganese oxidation state present in the monoclinic phase, the rhombohedral to monoclinic transition taking place at high temperature should produce, in this case, the reduction of Mn^{4+} to Mn^{3+}, with the consequent segregation of the manganese excess as manganese oxides. Nonetheless, no trace of the segregated phase was found after thermal treatments in powder XRD patterns. Therefore, since the presence of Mn^{4+} in the rhombohedral structure can be excluded, the $B1$ site symmetry and the corresponding interatomic distances could be consistent with the presence of a non active Jahn-Teller ion as Mn^{3+} in low spin electronic configuration. This characteristic has been observed in the rhombohedral perovskite $LaCoO_3$,[16] where the presence of the transition metal in low spin state forces the symmetry of the system to change from monoclinic to rhombohedral. Although this feature seems quite unusual in manganites, several low spin Mn^{3+} compounds are known. Beside a number of Mn^{III} complexes, very recently the Jahn-Teller suppression coupled with high-spin–low-spin transition was observed under pressure in $CsMnF_4$.[17] The possibility of the occurrence of a high-spin-low-spin transition in manganese compounds was studied long time ago on the basis of molecular orbital calculations for the $(MnO_6)^{n-}$ clusters.[18] Differently from the case of Mn^{2+}, for which the transition is unlikely, the smaller exchange splitting of the $2t_{2g}$ orbital and the larger crystal field splitting in the (MnO_6^{9-}) cluster suggest that a high-spin to low-spin transition of Mn^{3+} can occur. When the Mn-O distance is decreased under pressure, the low-spin configuration is found to be the most stable; this suggests that low-spin Mn^{3+} may substitute for Mn^{4+} in the manganese (IV) oxides, the ionic radii of Mn^{4+} and low spin Mn^{3+} being fairly similar.[19] This happens also under chemical pressure, when Mn^{4+} is substituted by the larger Zr^{4+} cation in the calcium manganite perovskite. The resulting solid solution is oxygen deficient $[Ca(Mn_{1-x}Zr_x)O_{3-\delta}, x \leq 0.07]$ since Mn^{4+} is progressively substituted by low spin Mn^{3+} by increasing the Zr content.[20] Since the energetically favored high-spin configuration of the Mn^{3+} ion is further stabilized via the Jahn-Teller distortion of its coordination environment, the presence of symmetry constrains that suppress the Jahn-Teller effect can lead to low-spin configuration: low-spin Mn^{3+} in rhombohedral $LiMnO_2$ was recently predicted by first-principles calculations.[21] Moreover, the presence of a low-spin ion, with a slightly smaller radius, would agree with the reduction in the Mn-O distance for the $B1$ site and with the increase in the tilt angle of the MnO_6 octahedra observed in the rhombohedral phase. Noteworthy is the indication of an unusual coexistence of manganese atoms in high- and low-spin configurations in the rhombohedral structure; to the authors' knowledge this feature has never been reported and deserves further verifications. However support to this hypothesis could be found in the irreversibility of the rhombohedral-monoclinic transition observed on heating at room pressure. From a structural point of view this transition, implying only a small distortion of the atomic arrangement, presents a displacive character that by itself, in absence of an external constrain, assures fast kinetics to both direct and reverse transition processes. However, since high pressure is required to stabilize low-spin state in Mn^{3+}, the monoclinic-rhombohedral transformation could be prevented at room pressure, when involving a high-low spin electronic transition.

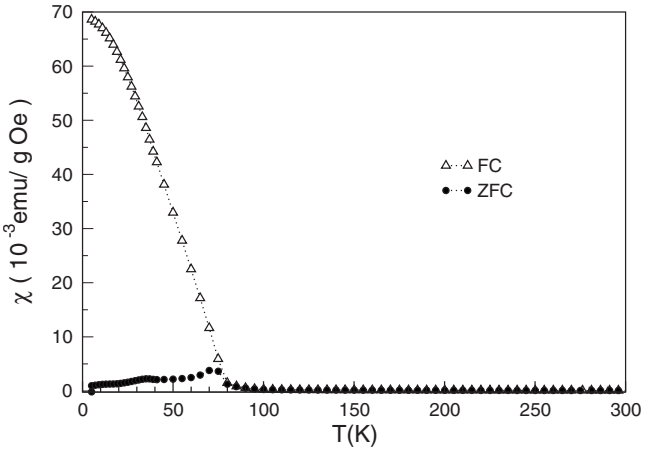

FIG. 5. Field cooled (FC) and zero field cooled (ZFC) magnetic susceptibility of $PrMn_7O_{12}$ in the monoclinic phase ($H=100$ Oe).

In any case, independently of the spin state of the manganese ions, it should be noted that the change in symmetry from monoclinic to rhombohedral invalidates the orbital ordering scheme previously proposed for the monoclinic structure, dramatically modifying the whole system of spin interactions and, reasonably, the magnetic properties of the compound.

Further support to the exclusive presence of Mn^{3+} in $PrMn_7O_{12}$ (that implies the presence of Pr^{3+}) was given by investigating the effect of the red-ox potential of the reagents on the reaction products. In fact we carried out a "three-capsules" synthesis ($P=40$ kbar, $T=1000$ °C), using respectively MnO_2 (Mn^{4+}), Mn_2O_3 (Mn^{3+}), and MnO (Mn^{2+}) as reagent oxide, mixed with Pr_6O_{11} in stoichiometric ratio. While the capsule with the "standard" reagent (Mn_2O_3) resulted in the expected $PrMn_7O_{12}$ phase, in the other cases we did not find any trace of $PrMn_7O_{12}$: the products contained a large fraction of unreacted Mn-oxides, $PrMnO_3$ and Pr_6O_{11}.

C. Magnetic properties

The magnetic properties of $PrMn_7O_{12}$ have been studied using a SQUID magnetometer. In Figs. 5 and 6 the dc magnetic susceptibility of samples of the monoclinic and rhombohedral phases, respectively, is reported, where the most striking feature is the totally different behavior of samples of the two phases. While monoclinic samples exhibit a regular magnetic transition at temperature, evaluated from the inflection point, at $T_c \cong 70$ K with weak magnetic moment of $\cong 0.07$ emu/g Oe in the ordered state at $T=5$ K and $H=100$ Oe, in the rhombohedral samples the magnetic transition occurs at $T_c \cong 44$ K, with a characteristic bump below T_c and magnetic moment in the ordered phase about 2 orders of magnitude weaker with respect to the monoclinic samples. Field cooled inverse magnetic susceptibilities, shown in Fig.

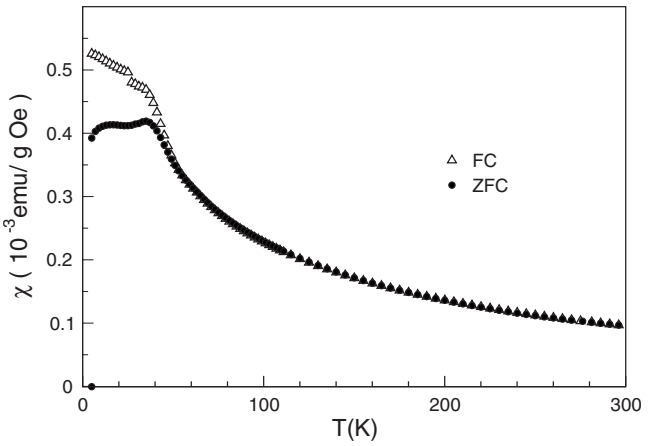

FIG. 6. Field cooled (FC) and zero field cooled (ZFC) magnetic susceptibility of $PrMn_7O_{12}$ in the rhombohedral phase (H = 100 Oe).

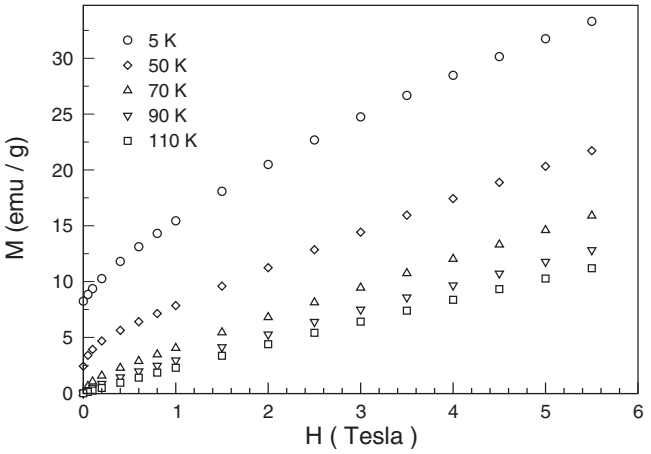

FIG. 8. Field dependence of magnetization of $PrMn_7O_{12}$ in the monoclinic phase at selected temperatures.

7, points to antiferromagnetic behavior for both phases. The slope in the paramagnetic region yields an average moment of $4.73\mu_B$ and $4.54\mu_B$ per magnetic ion (Pr^{3+} included) for the monoclinic and the rhombohedral phases, respectively, in good agreement with the calculated value of $4.75\mu_B$ per high spin magnetic ion (Pr^{3+} included), and the corresponding Curie Weiss temperatures are 53 and 30 K. In light of these results, the magnetization of the monoclinic phase can be likely ascribed to orbital ordering with A-AFM magnetic structure and Dzyaloshinsky-Moryia (DM) interaction, originating in the tilting of the Jahn-Teller distorted MnO_6 octahedra. In fact the DM interaction can be inferred from the two following remarks. First, the inverse susceptibility (Fig. 7) exhibits a sharp drop at the transition temperature: this peculiar shape differs from the usual behavior of antiferromagnets, and is observed in pure DM compounds.[22,23] Second, the isotherm magnetization curves below T_c in Fig. 8 show zero field remanence; this too is not normal for antiferromagnets, where one usually observes straight lines passing through the axes origin, and it has been shown[24] that can be ascribed to the DM interaction. Different origin of the remanence, such as strong competing anisotropies can be ruled out by the observed negligible coercitive field. For the rhombohedral phase, conversely, both inverse susceptibility and isotherm magnetization curves behave as for a normal antiferromagnet, pointing to the lack of DM interaction. The peak corresponding to the Néel temperature is probably disguised by magnetic Mn oxide impurities, mainly antiferromagnetic Mn_2O_3 and ferrimagnetic Mn_3O_4 (indeed[25] Mn_3O_4 is a ferrimagnet with $T_c \cong 43$ K, whose magnetic susceptibility shows a bump below T_c similar to those appearing in Fig. 6). However, even a different contribution of Pr to the magnetic ordering could be taken into account. This difference in the magnetic behavior is observed also in the samples thermally treated: the high-temperature rhombohedral to monoclinic transition previously characterized by the structural point of view is clearly observed by susceptibility measures as a two order change of magnetization at 5 K. A possible origin for the different magnetic properties of the two phases could be the change in spin configuration previously hypothesized. In fact, according to ligand field theory, the four electrons of the octahedrically coordinated Mn^{3+} ions may in principle arrange in high-spin (S=2), low-spin (S=1) and nonspin (S=0) configuration. The high-spin state would be the ground state for the monoclinic phase inducing Jahn-Teller distortion and DM interaction, while the low-spin (or even nonspin) state would be the ground state for the rhombohedral phase and Jahn Teller distortion would be absent: this kind of mechanism has already been observed in other transition-metal oxides, for instance in $LiMnO_2$ (Ref. 21) or in $LaCoO_3$.[26] Although the obtained experimental values of Bohr magnetons for the monoclinic phase (with Pr^{3+} and Mn^{3+} all high spin) and the rhombohedral phase (with only one Mn^{3+} low spin, S=1) are close to the theoretical ones, validation of the hypothesis concerning the coexistence of high- and low-spin Mn atoms in the same structure is not possible within the frame of the presently available data. In fact, taking into account the Pr^{3+} contribution, the paramagnetic moments calculated by considering one Mn^{3+} ion per f.u. in high-, low- or nonspin states are $4.75\mu_B$, $4.53\mu_B$, and $4.42\mu_B$, respectively, too similar to assign unambiguously the spin state on the basis of the measured inverse magnetic

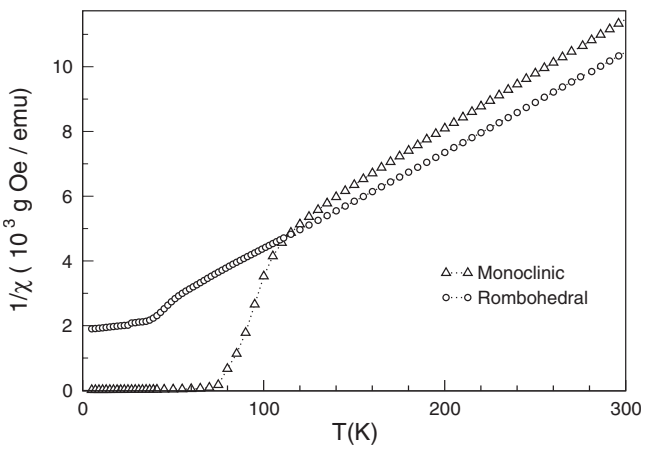

FIG. 7. Field cooled inverse magnetic susceptibility for $PrMn_7O_{12}$ in the monoclinic and rhombohedral phase. The slopes in the paramagnetic region yield $4.73\mu_B$ and $4.54\mu_B$ per magnetic ion.

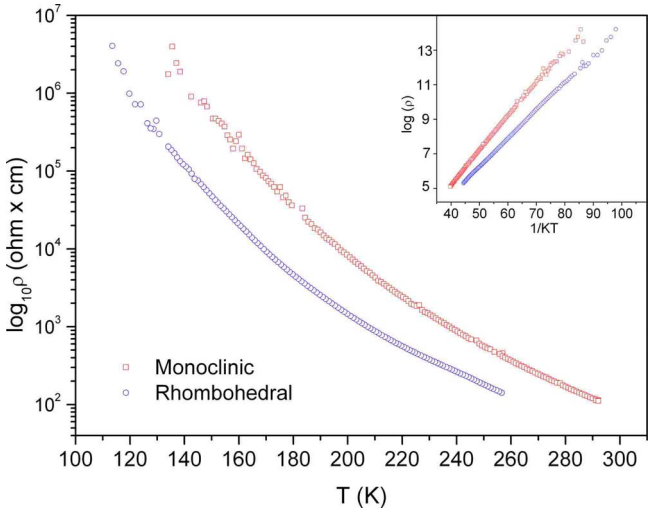

FIG. 9. (Color online) dc electrical resistivity vs temperature for $PrMn_7O_{12}$ polymorphs.

susceptibilities shown in Fig. 6. A detailed structural analysis (neutron diffraction) and spectroscopic studies (electronic paramagnetic resonance) are needed in order to clarify the magnetic structure, the contribution of Pr to the magnetic ordering and the Mn electronic configuration.

D. Transport properties

dc resistivity $R(T)$ has been measured by standard four-probe method from 100 to 300 K using a close cycle cryostat. $PrMn_7O_{12}$ shows semiconducting behavior (Fig. 9), with high sample resistance and capacitive component preventing reliable values at $T<100$ K; however no transition occurs in the range 100 K-RT. The activation energies measured from the resistivity Arrhenius plot are 220 and 170 meV for the monoclinic and the rhombohedral phases, respectively (Fig. 9, inset). The lower energy of the rhombohedral phase could be explained with the occupation of the spin down state in the t_{2g} band giving an increase in conductivity as reported for half-metal materials such as $LiMnO_2$.[21] The energy activation is significantly larger than those of structurally similar materials, such as $NaMn_7O_{12}$ (50 meV),[1] or $LaMn_7O_{12}$ (96 meV).[3]

IV. CONCLUSIONS

A new metastable complex manganite with formula $PrMn_7O_{12}$ and perovskite-type structure has been synthesized in HP/HT conditions; it crystallizes in two phases with monoclinic and rhombohedral symmetry, for which the phase diagram and the stability region in the P/T space have been defined. Whereas the monoclinic phase is strongly related to $LaMn_7O_{12}$ in terms of structure and orbital orderings, the rhombohedral phase adopts the structure of $CaMn_7O_{12}$, which typically allows to accommodate Mn^{4+} and Mn^{3+} in the B sites of this complex perovskite in a stoichiometric 1:3 ratio. Structural characterization indicates in both structures the sole presence of Mn^{3+} and suggests the presence, in the rhombohedral polymorph, of manganese in both high- and low-spin configuration, which might account for the dramatic difference observed in the magnetic properties of the two phases. The low spin manganese would occupy the undistorted octahedral site of the rhombohedral structure, Jahn-Teller inactive by symmetry constrains, which is occupied by Mn^{4+} in the corresponding calcium compound.

ACKNOWLEDGMENTS

The authors wish to express their acknowledgments to M. Marezio, A. Prodi, A. Gauzzi, F. Licci, and A. Daoud-Aladin for fruitful discussions, T. Besagni for XRD, P. Ferro for samples preparation, and G. Gnappi for DSC measurements. A few high pressure experiments of $PrMn_7O_{12}$ were performed at the Bayerisches Geoinstitut at Bayreuth under the EU "Research Infrastructures: Transnational Access" Programme [Contract No. 505320 (RITA)—high pressure].

*Corresponding author. Fax:+39 0521 905556; francesco.mezzadri@nemo.unipr.it

[1] A. Prodi, E. Gilioli, A. Gauzzi, F. Licci, M. Marezio, F. Bolzoni, Q. Huang, A. Santoro, and J. W. Lynn, Nature Mater. **3**, 48 (2004).
[2] B. Bochu, J. Chenavas, C. Joubert, and M. Marezio, J. Solid State Chem. **11**, 88 (1974).
[3] A. Prodi, Q. Huang, A. Santoro, J. W. Lynn, M. Affronte, M. Marezio, A. Gauzzi, F. Licci, R. Cabassi, F. Bolzoni, and E. Gilioli (unpublished).
[4] M. N. Deschizeaux, J. C. Joubert, A. Vegas, A. Collomb, J. Chenavas, and M. Marezio, J. Solid State Chem. **19**, 45 (1976).
[5] V. M. Goldschmidt, Naturwiss. **14**, 477 (1926).
[6] J.-S. Zhou and J. B. Goodenough, Phys. Rev. B **68**, 054403 (2003).
[7] A. Collomb, D. Samaras, G. Fillion, M. N. Deschizeaux, and J. C. Joubert, J. Magn. Magn. Mater. **8**, 77 (1978).
[8] E. Gilioli, G. Calestani, F. Licci, C. Paorici, A. Gauzzi, F. Bolzoni, and A. Prodi, J. Solid State Chem. **179**, 3839 (2006).
[9] A. C. Larson and R. B. Von Dreele, Los Alamos National Laboratory Report No. LAUR 86-748, 2000 (unpublished).
[10] V. V. Brazhkin, arXiv:cond-mat/0605626 (unpublished).
[11] A. Altomare, M. C. Burla, M. Camalli, G. Cascarano, C. Giacovazzo, A. Guagliardi, A. G. G. Moliterni, G. Polidori, and R. Spagna, *SIR2002, Program for Crystal Structure Solution and Refinement* (IRMEC-CNR, Bari, Italy, 2002).
[12] G. M. Sheldrick, *SHELXL93, Program for the Crystal Structure Refinement* (University of Gottingen, Germany, 1993).
[13] H. B. Toby, J. Appl. Crystallogr. **34**, 210 (2001).
[14] M. Nespolo, G. Ferraris, and H. Ohashi, Acta Crystallogr., Sect. B: Struct. Sci. **55**, 902 (1999).
[15] E. O. Wollan and W. C. Koeler, Phys. Rev. **100**, 545 (1955).

[16] G. Maris, Y. Ren, V. Volotchaev, C. Zobel, T. Lorenz, and T. T. M. Palstra, Phys. Rev. B **67**, 224423 (2003).
[17] F. Aguado, F. Rodriguez, and P. Núñez, Phys. Rev. B **76**, 094417 (2007).
[18] D. M. Sherman, Am. Mineral. **69**, 788 (1984).
[19] R. D. Shannon and C. T. Prewitt, Acta Crystallogr., Sect. B: Struct. Crystallogr. Cryst. Chem. **25**, 925 (1969).
[20] H. Taguchi, K. Hirota, S. Nishihara, S. Morimoto, K. Takaoka, M. Yoshinaka, and O. Yamaguchi, Physica B **367**, 188 (2005).
[21] Z.-F. Huang, F. Du, C.-Z. Wang, D.-P. Wang, and G. Chen, Phys. Rev. B **75**, 054411 (2007).
[22] J. TÖpfer and J. B. Goodenough, J. Solid State Chem. **130**, 117 (1997).
[23] J. Hemberger, F. Schrettle, A. Pimenov, P. Lunkenheimer, V. Y. Ivanov, A. A. Mukhin, A. M. Balbashov, and A. Loidl, Phys. Rev. B **75**, 035118 (2007).
[24] F. Bolzoni and R. Cabassi, J. Appl. Phys. **103**, 063905 (2008).
[25] M. S. Jagadeesh and Mohindar S. Seehra, Phys. Rev. B **21**, 2897 (1980).
[26] C. Zobel, M. Kriener, D. Bruns, J. Baier, M. Grüninger, T. Lorenz, P. Reutler, and A. Revcolevschi, Phys. Rev. B **66**, 020402(R) (2002).
[27] M. W. Lufaso and P. M. Woodward, Acta Crystallogr., Sect. B: Struct. Sci. **60**, 10 (2004).